

Characterization of magnetic properties, including magnetocaloric effect, of $\text{RE}_5\text{Pt}_2\text{In}_4$ (RE = Gd-Tm) compounds

Altifani Rizky Hayyu,^{1,*} Stanisław Baran,^{1,†} and Andrzej Szytuła¹

¹*M. Smoluchowski Institute of Physics, Jagiellonian University,
prof. Stanisława Łojasiewicza 11, PL-30-348 Kraków, Poland*

(Dated: April 26, 2023)

The $\text{RE}_5\text{Pt}_2\text{In}_4$ (RE = Gd-Tm) rare earth compounds have been investigated by means of X-ray diffraction (XRD) as well as by DC and AC magnetometric measurements. The compounds crystallize in an orthorhombic crystal structure of the $\text{Lu}_5\text{Ni}_2\text{In}_4$ -type ($Pbam$ space group, No. 55). With decreasing temperature the intermetallics undergo a transition from para- to ferro-/ferri- (RE = Gd, Tb, Ho, Er) or antiferromagnetic state (RE = Tm). In case of $\text{Dy}_5\text{Pt}_2\text{In}_4$, the ferromagnetic state is reached through an intermediate antiferromagnetic order present in a limited temperature range. The critical temperatures of magnetic ordering range from 4.1 K (RE = Tm) up to 108 K (RE = Tb). For the majority of investigated compounds, a cascade of additional magnetic transitions is found below the respective critical temperatures of magnetic ordering. The magnetic moments are found solely on the rare earth atoms, while the moments of the remaining Pt and In atoms are absent or are too small to be detected while accompanied by the strong rare earth's moments. The magnetocaloric (MCE) performance of $\text{RE}_5\text{T}_2\text{In}_4$ (RE = Gd-Tm) is found quite good, especially while taking into account the compounds with RE = Ho and Er. Maximum magnetic entropy change ($-\Delta S_M^{max}$) reaches 11.8 (RE = Ho) or 11.4 $\text{J}\cdot\text{kg}^{-1}\cdot\text{K}^{-1}$ (RE = Er) under magnetic flux density change of 0-9 T. Under the same conditions, the relative cooling power (RCP) and refrigerant capacity (RC) equal 607 and 495 $\text{J}\cdot\text{kg}^{-1}$ (RE = Ho) or 434 and 341 $\text{J}\cdot\text{kg}^{-1}$ (RE = Er).

keywords: rare earth intermetallics, magnetic properties, magnetization, magnetocaloric effect, magnetic entropy change, relative cooling power

I. INTRODUCTION

Rare earth intermetallic compounds have been attracting researchers' interest due to a number of intriguing physical phenomena including multiple magnetic transitions, metamagnetism, large magnetocaloric effect (MCE), spin glass state, heavy fermion behavior, superconductivity, and many more. A review paper by Gupta and Suresh [1], reporting the current state of knowledge for the RTX (R = rare earths, T = Sc, Ti, Mn, Fe, Co, Ni, Cu, Ru, Rh, Pd, Ag, Os, Ir, Pt, Au, and X = Al, Ga, In, Si, Ge, Sn, As, Sb, Bi) series of intermetallics, may provide an idea of the multitude of interesting phenomena observed in rare earth intermetallic compounds.

Nowadays, the compounds with complex crystal structure and magnetic properties resulting from multiple magnetic sublattices are of particular interest. The $\text{RE}_5\text{Pt}_2\text{In}_4$ (RE = Gd-Tm) indides are a good example of such a family of compounds, as they crystallize in an orthorhombic structure of the $\text{Lu}_5\text{Ni}_2\text{In}_4$ -type ($Pbam$ space group, No. 55) [2]. In this structure, reported for the first time by Zaremba et al. [3], the rare earth atoms occupy three different Wyckoff sites, namely, the 2(a) site and two 4(g) sites with different atomic positional parameters.

Up to now magnetic properties of $\text{RE}_5\text{Pt}_2\text{In}_4$ (RE = Gd-Tm) remain unexplored. However, such properties

including magnetic structures, have been reported for the isostructural $\text{RE}_5\text{Ni}_2\text{In}_4$ [4–10] and $\text{RE}_5\text{Pd}_2\text{In}_4$ [11] (RE = Tb-Tm). Both the Ni- and Pd-based intermetallics are found to order magnetically at low temperatures with the critical temperatures of magnetic ordering ranging from about 4 K in the Tm-based compounds up to 125 K reported for $\text{Tb}_5\text{Ni}_2\text{In}_4$. The magnetic moments are carried solely by the rare earth atoms (Ni, Pd and In remain non-magnetic or have magnetic too small to be detectable in presence of the strong rare earth moments). Below the respective critical temperature, a cascade of temperature-induced magnetic transitions is observed for most of the compounds. Neutron diffraction data reveal that these complex magnetic properties can be attributed to either different ordering temperatures in different rare earth sublattices or order-order magnetic transitions. The low-temperature magnetic structures show a variety of forms including ferro- and antiferromagnetic spin arrangements, as well as the coexistence of both types of ordering in selected compounds. The reported magnetic structures include both commensurate and incommensurate ones.

Magnetocaloric effect (MCE) in the rare earth-based compounds is recently of great interest due to possible applications in refrigeration [12–22]. It is until now that MCE in the $\text{RE}_5\text{T}_2\text{In}_4$ (RE = rare earth element; T = transition metal) intermetallics has only been reported for $\text{RE}_5\text{Ni}_2\text{In}_4$ (RE = Dy, Ho, and Er) [10]. It has been found that for RE = Ho and Er, the maximum entropy changes exceed 10 $\text{J}\cdot\text{kg}^{-1}\cdot\text{K}^{-1}$ under magnetic flux change 0-7 T. The maximum entropy changes are

* altifani.hayyu@doctoral.uj.edu.pl

† stanislaw.baran@uj.edu.pl

reached in the vicinity of the respective Curie temperatures, which are close to 20 K.

Complex magnetic properties, reported for the isostructural $\text{RE}_5\text{Ni}_2\text{In}_4$ and $\text{RE}_5\text{Pd}_2\text{In}_4$ ($\text{RE} = \text{Tb-Tm}$), has inspired us to undertake the current study concentrated on $\text{RE}_5\text{Pt}_2\text{In}_4$ ($\text{RE} = \text{Gd-Tm}$). We report here not only the basic magnetic properties, like magnetic transition temperatures, effective magnetic moments, the moments under applied magnetic field, critical and coercivity fields, etc., but also we report the magnetocaloric effect studied under magnetic flux change up to 0-9 T. As a result, we determine the number of parameters important from the point of view of potential application in a low-temperature refrigeration. The parameters include temperature averaged magnetic entropy change (TEC), relative cooling power (RCP), and refrigerant capacity (RC). The experimental results reported in this work are compared with those reported previously for the isostructural $\text{RE}_5\text{Ni}_2\text{In}_4$ and $\text{RE}_5\text{Pd}_2\text{In}_4$ ($\text{RE} = \text{Tb-Tm}$).

II. MATERIALS AND METHODS

The samples have been prepared by arc melting of high-purity elements (at least 99.9 wt %) under titanium-gettered argon atmosphere. The elements have been taken in a stoichiometric ratio. The obtained ingots have been remelted a few times in order to improve their homogeneity. No annealing have been applied as our previous tests have shown that annealing leads to the appearance of impurity phases. The crystal structure of the obtained samples has been examined by X-ray powder diffraction at room temperature using a PANalytical X'Pert PRO diffractometer (Cu $K\alpha$ radiation, Bragg-Brentano geometry, measured angle interval of $2\theta = 10 - 100^\circ$, 2θ step = 0.033° , 150 s/step). The X-ray diffraction data have been processed using the FullProf program package [23, 24].

For the DC and AC magnetic measurements, the powder samples have been encapsuled in plastic containers and glued by varnish in order to prevent grain rotation or movement during the measurement. A Vibrating Sample Magnetometer (VSM) option of the Physical Properties Measurement System (PPMS) by Quantum Design has been utilized for DC magnetic measurements. Magnetic susceptibility data have been collected over a wide temperature range of 1.85–390 K using both the Zero Field Cooling (ZFC) and Field Cooling (FC) regimes. Every time before collecting a ZFC curve, the sample has been heated to a temperature exceeding the respective critical temperature of magnetic ordering, then demagnetized by the oscillating magnetic field, and finally cooled down to 1.9 K. The ZFC and FC collected at a low magnetic field of 50 Oe have been used to determine magnetic transition temperatures, while from the ZFC data taken at 1 kOe the effective magnetic moments (μ_{eff}) and paramagnetic Curie temperatures (θ_p) have been derived. In order to follow the thermal evolution of magnetic order, isothermal magnetization curves have been collected in

magnetic fields up to 90 kOe (9 T) at a number of selected temperatures. Before collecting a magnetization curve, the sample has been demagnetized using the described above procedure.

AC magnetic susceptibility measurements have been performed using an AC Measurement System (ACMS) option of PPMS. The data have been collected under an oscillating magnetic field of 2 Oe amplitude at a number of selected frequencies between 100 and 5000 Hz. The temperature interval has covered 1.9–300 K.

The crystal structure has been visualized (see Fig. 1 with the use of the VESTA program [25].

III. RESULTS

A. Crystal structure

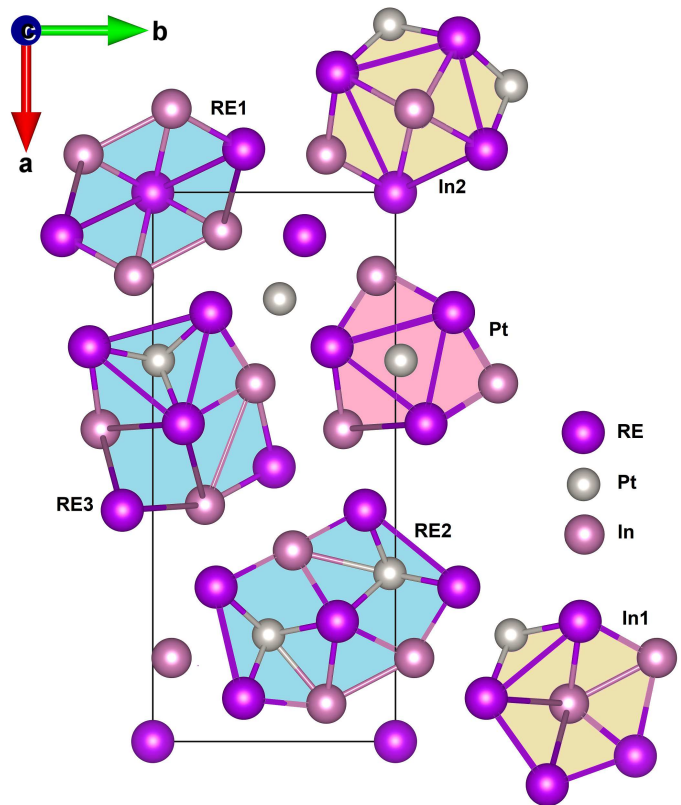


FIG. 1. Perspective view of the crystal structure of $\text{RE}_5\text{Pt}_2\text{In}_4$ showing its layered nature.

X-ray powder diffraction data collected for the $\text{RE}_5\text{Pt}_2\text{In}_4$ ($\text{RE} = \text{Gd-Tm}$) samples at room temperature confirm that the compounds crystallize in an orthorhombic crystal structure of the $\text{Lu}_5\text{Ni}_2\text{In}_4$ -type (Pearson symbol oP22, space group $Pbam$, No. 55, $Z = 2$). This result is in agreement with the previous report [2]. The $\text{Lu}_5\text{Ni}_2\text{In}_4$ -type structure consists of distorted trigonal and square prismatic slabs of the REPt and REIn compositions [3]. The structure is a layered-one with atoms

situated on the mirror planes at $z = 0$ and $z = \frac{1}{2}$. The layers formed by the rare earth atoms are separated by the layers containing Pt and In (see Fig. 1). The rare earth atoms occupy three different Wyckoff sites, namely, one 2a site (0,0,0) and two 4g sites ($x, y, 0$) with different atom positional parameters. The Pt atoms occupy one 4h site ($x, y, \frac{1}{2}$), while the In atoms are located at two other 4h sites with different atom positional parameters.

Fig. 2 shows X-ray powder diffraction patterns of $\text{RE}_5\text{Pt}_2\text{In}_4$ (RE = Gd-Tm) collected at room temperature, together with the results of Rietveld refinement. The refined parameters of the crystal structure are listed in Table I.

B. Magnetic properties

1. DC and AC magnetic susceptibility data

The results of DC magnetic measurements of $\text{RE}_5\text{Pt}_2\text{In}_4$ (RE = Gd-Tm) are presented in Fig. 3 and summarized in Table II. At a low magnetic field of 50 Oe, all compounds show transitions from para- to magnetically ordered state with decreasing temperature, namely, for RE = Gd, Tb, Ho and Er a rapid increase of magnetic susceptibility, characteristic of para- to ferromagnetic transition, is visible, while for RE = Tm a maximum typical of para- to antiferromagnetic transition is found (see the upper insets in Figs. 3a-f). The case of $\text{Dy}_5\text{Pt}_2\text{In}_4$ is more complicated as the ferromagnetic transition at $T_C = 80$ K is preceded by an intermediate antiferromagnetic state manifesting itself by a maximum at $T_N = 93$ K. Below the critical temperatures of magnetic ordering, a number of additional magnetic transitions are detected from either additional maxima or inflection points. The magnetic transition temperatures are listed in Table II. Large discrepancies between the ZFC and FC curves, visible especially for RE = Gd-Ho below the corresponding Curie temperatures, are magnetic domains-related effects, indicating presence of a ferromagnetic component of the magnetic order. The discrepancy found for RE = Tm, both below and above the Néel temperature of 4.1 K, can be attributed to a very small amount of ferromagnetic impurity phase, whose content is too small to be detectable by other experimental techniques like X-ray powder diffraction (XRD).

The maxima visible in the AC magnetic susceptibility vs. temperature curves (see Fig. 4) coincide with the magnetic transition temperatures derived from the DC magnetic data (see Table II). Some discrepancies between the DC and AC data can be attributed to different experimental conditions, namely, the AC data have been collected under the oscillating field of 2 Oe and no applied DC field, while the DC data have been recorded under a constant field of 50 Oe. Although relatively low, the latter field may influence temperatures of magnetic transition sensitive to the applied magnetic field. It is worth noting that for $\text{Dy}_5\text{Pt}_2\text{In}_4$, the Néel temperature

derived from the DC data coincides with a distinct maximum observed in χ'_{ac} at 93 K (there is no anomaly at this temperature in χ''_{ac}), while the Curie point of 80 K is accompanied by maxima in both χ'_{ac} and χ''_{ac} .

The reciprocal magnetic susceptibility curves, collected at $H = 1$ kOe, become linear at high-enough temperatures as predicted by the Curie-Weiss law [26]:

$$\chi = \frac{C}{T - \theta_p} \quad (1)$$

where C is the Curie constant related to the effective magnetic moment (μ_{eff}), while θ_p is a paramagnetic Curie temperature. The values of μ_{eff} and θ_p , as derived from fitting the linear dependence to $\chi_{dc}^{-1}(T)$ at high temperature regions, are listed in Table II. The values of μ_{eff} are very close to those predicted for the free RE^{3+} ions. It is worth noting that for all investigated compounds, the determined paramagnetic Curie temperatures are positive, indicating the predominant role of the ferromagnetic interactions.

2. Magnetization

The lower insets in Figs. 3a-f show magnetization curves for $\text{RE}_5\text{Pt}_2\text{In}_4$ (RE = Gd-Tm) taken in applied magnetic fields up to 90 kOe at a number of selected temperatures. The shape of the curves, especially those collected at lower temperatures, testifies to the coexistence of ferro- and antiferromagnetic components of the magnetic structures as both metamagnetic transitions as well as magnetic hysteresis are observed. The critical fields, corresponding to the metamagnetic transitions, have been determined from inflection points in the primary magnetization curves, i.e. the curves recorded directly after the zero-field cooling (ZFC) procedure. The values of critical fields derived from experimental data are listed in Table II. The appearance of metamagnetic transition confirms the existence of an antiferromagnetic component, which is suppressed by application of a high-enough external magnetic field. The ferromagnetic component of the magnetic structure manifests itself in non-zero coercivity field. The observed values of coercivity fields are also reported in Table II.

It is worth noting that both the Tb- and Dy-based compounds show very high values of critical and coercivity fields at 1.9 K, testifying to stronger magnetic interactions than in the other investigated compounds. Such a result coincides with the highest ordering temperatures observed for RE = Tb and Dy.

The case of $\text{Dy}_5\text{Pt}_2\text{In}_4$ is very special as the critical field initially decreases with increasing temperature, reaching 0.1 kOe at 75 K, and afterward increases again to 0.5 kOe at 87 K. Such a result is in agreement with the susceptibility data (see subsection III B 1), which suggest suppression of the ferromagnetic component of the $\text{Dy}_5\text{Pt}_2\text{In}_4$ magnetic structure at $T_C = 80$ K with further

TABLE I. Crystallographic data obtained from Rietveld refinement of the X-ray powder diffraction patterns collected at room temperature for RE₅Pt₂In₄ (RE = Gd-Tm; Lu₅Ni₂In₄-type structure, space group *Pbam*, No. 55). The agreement factors $R_{profile}$, R_F , R_{Bragg} , and χ^2 characterizing quality of refinements are listed at the bottom of the table.

RE	Gd	Tb	Dy	Ho	Er	Tm
a [Å]	18.2045(20)	18.1218(14)	18.0551(13)	17.9991(15)	17.9447(11)	17.8935(18)
b [Å]	8.0461(9)	8.0140(6)	7.9886(5)	7.9731(6)	7.9524(5)	7.9212(8)
c [Å]	3.6771(5)	3.6500(5)	3.6270(3)	3.6115(4)	3.5942(2)	3.5776(5)
V [Å ³]	538.61(23)	530.08(16)	523.13(14)	518.28(16)	512.92(12)	507.08(20)
RE1 at 2a (0, 0, 0)	0	0	0	0	0	0
RE2 at 4g (x, y, 0)	$x = 0.2181(10)$ $y = 0.2394(28)$	0.2192(8) 0.2459(21)	0.2200(7) 0.2399(19)	0.2180(9) 0.2389(24)	0.2190(7) 0.2470(18)	0.2184(8) 0.2471(23)
RE3 at 4g (x, y, 0)	$x = 0.4204(12)$ $y = 0.1238(21)$	0.4181(10) 0.1215(17)	0.4168(8) 0.1150(15)	0.4215(11) 0.1196(19)	0.4168(7) 0.1244(14)	0.4181(9) 0.1218(18)
Pt at 4h (x, y, $\frac{1}{2}$)	$x = 0.3056(8)$ $y = 0.0217(20)$	0.3031(6) 0.0236(13)	0.3028(5) 0.0265(12)	0.3043(6) 0.0259(14)	0.3044(5) 0.0257(12)	0.3012(8) 0.0295(17)
In1 at 4h (x, y, $\frac{1}{2}$)	$x = 0.5695(14)$ $y = 0.2152(26)$	0.5678(9) 0.2102(17)	0.5645(8) 0.2175(17)	0.5652(10) 0.2111(17)	0.5691(9) 0.2056(15)	0.5606(11) 0.2094(19)
In2 at 4h (x, y, $\frac{1}{2}$)	$x = 0.8459(14)$ $y = 0.0753(27)$	0.8494(10) 0.0759(18)	0.8492(9) 0.0748(18)	0.8511(11) 0.0714(20)	0.8484(8) 0.0778(18)	0.8516(12) 0.0759(24)
$R_{profile}$ [%]	2.76	3.07	2.40	3.59	3.07	4.39
R_F [%]	8.19	9.55	6.08	6.71	4.88	5.95
R_{Bragg} [%]	12.5	11.3	9.34	10.9	6.96	9.70
χ^2	7.30	6.87	6.46	10.4	8.14	16.3

TABLE II. Parameters characterizing magnetic order: T_C (Curie temperature), T_N (Néel temperature), T_t (temperatures of additional anomalies), θ_p (paramagnetic Curie temperature), μ_{eff} (effective magnetic moment), $\mu[\mu_B]$ (magnetic moment in the ordered state), $H_{cr}[kOe]$ (the critical field) and $H_{coer}[kOe]$ (the coercivity field) for RE₅Pt₂In₄ (RE = Gd-Tm), as derived from DC and/or AC magnetometric measurements. The i and m indices indicate whether the transition temperature corresponds to an inflection point or to a maximum in the $\chi(T)$ curve, respectively. The transition temperatures are calculated from the ZFC data, except few cases based on the FC data and marked explicitly by an additional index f .

RE	T_C [K]			T_N [K]			T_t [K]			θ_p [K]	$\mu_{eff}[\mu_B]$		$\mu[\mu_B]$		$H_{cr}[kOe]$	$H_{coer}[kOe]$	
	χ_{dc}	χ'_{ac}	χ''_{ac}	χ_{dc}	χ'_{ac}	χ''_{ac}	χ_{dc}	χ'_{ac}	χ''_{ac}		Exp.	Theor.	Exp.	Theor.			
Gd	76 ⁱ	74 ^m	73 ^m				22.5 ⁱ				+72	7.87	7.94	3.86	7.00	T = 1.9 K: 0.16 T = 40.0 K: 0.05 T = 68.0 K: 0.02	0.11 0.02
Tb	108 ⁱ	106 ^m	104 ^m				83 ⁱ				+48	9.55	9.72	4.34	9.00	T = 1.9 K: 44 T = 20.0 K: 1.7 T = 100.0 K: 0.03	23.7 1.9
Dy	80 ⁱ	84 ^m	80 ^m	93 ^m	93 ^m		19.6 ^{m,f} , 71 ⁱ	14.1 ^m			+24.6	10.61	10.65	5.74	10.00	T = 1.9 K: 24.3, 45 T = 12.0 K: 13.5 T = 25.0 K: 2.2 T = 75.0 K: 0.1 T = 87.0 K: 0.5	22.1 11.5 2.4 0.03
Ho	23.5 ⁱ	22.7 ^m	22.1 ^m				9.1 ^{m,f} , 13.5 ⁱ	8.1 ^m			+10.1	10.62	10.61	6.98	10.00	T = 1.9 K: 2.9 T = 9.0 K: 0.22 T = 15.0 K: 0.08 T = 20.0 K: 0.02	1.4 0.23 0.03
Er	12.6 ⁱ	12.1 ^m	11.9 ^m				6.9 ⁱ , 8.8 ⁱ		7.1 ^m	+11.1	9.44	9.59	3.24	9.00	T = 1.9 K: 0.96 T = 7.0 K: 0.21 T = 9.5 K: 0.08	0.3 0.09 0.02	
Tm				4.1 ^m	4.2 ^m	4.2 ^m				+4.6	7.45	7.57	3.54	7.00	T = 1.9 K: 9.2 T = 3.0 K: 7.6 T = 4.0 K: 0.07	0.03 0.04 0.02	

i – inflection point; m – maximum; f – determined from the FC curve

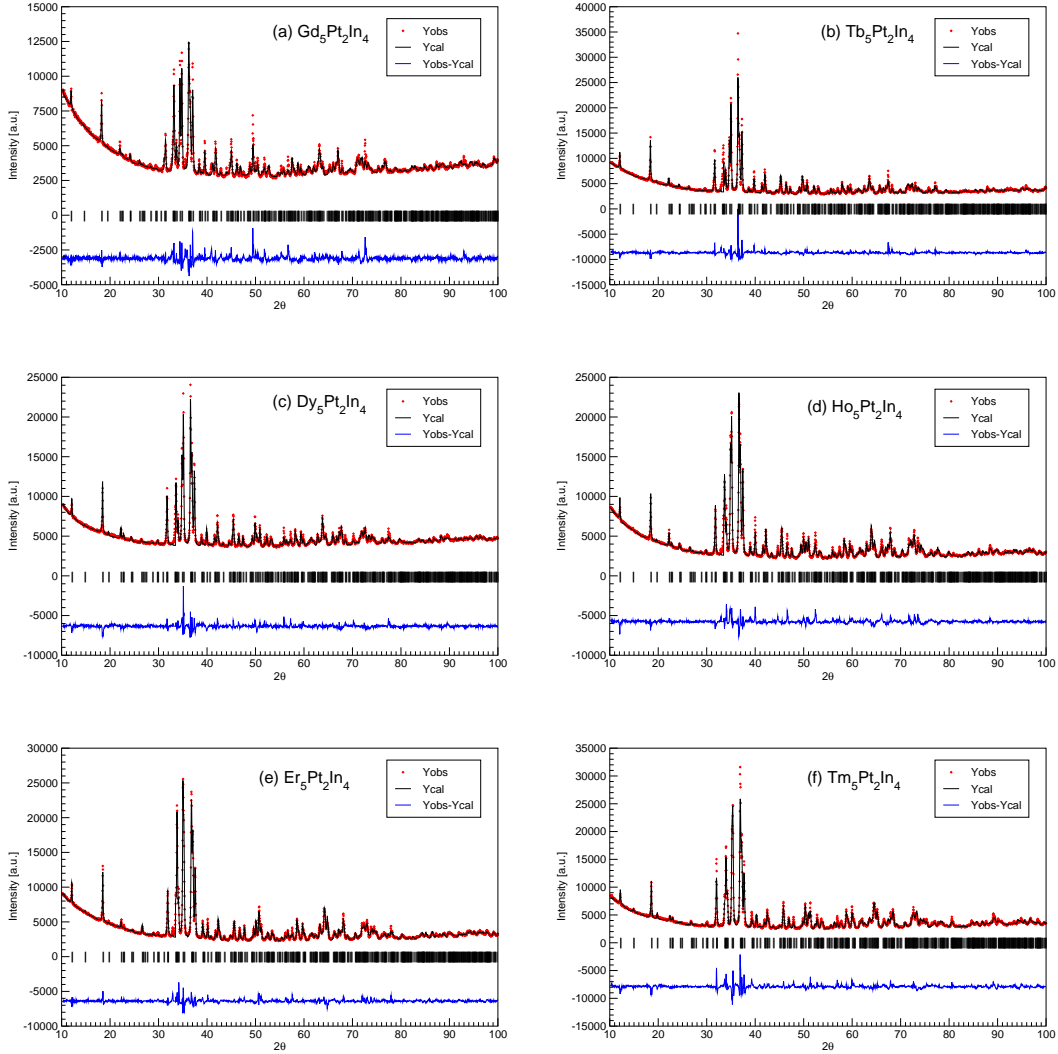


FIG. 2. X-ray diffraction patterns collected at room temperature for $\text{RE}_5\text{Pt}_2\text{In}_4$: (a) $\text{RE} = \text{Gd}$, (b) $\text{RE} = \text{Tb}$, (c) $\text{RE} = \text{Dy}$ (d) $\text{RE} = \text{Ho}$, (e) $\text{RE} = \text{Er}$ and (f) $\text{RE} = \text{Tm}$. The solid circles denote the experimental data, while the black lines show the Rietveld refinement results. The vertical bars indicate Bragg reflection positions, whereas the difference between the experimental data and the refinement is presented as the blue line at the bottom of each subfigure.

development of the antiferromagnetic one, which exists up to $T_N = 93$ K.

The determined values of the magnetic moments in the ordered state, as derived from magnetization data taken at 1.9 K and 90 kOe, are significantly lower than the values expected for free RE^{3+} ions (for example, for $\text{Tb}_5\text{Pt}_2\text{In}_4$ it is $4.34 \mu_B$, which is only 48 % of the theoretical value for Tb^{3+} which equals $9.00 \mu_B$ – for other compounds, see Table II). Nevertheless, one should take into account that the magnetization curves collected at 1.9 K are far away from saturation even at a relatively high magnetic field of 90 kOe.

3. Magnetocaloric effect

a. Magnetic entropy change and temperature averaged magnetic entropy change (TEC)

Considering the magnetic entropy (S_M) as a function of magnetic flux density ($\mu_0 H$) and temperature (T), its differential dS_M can be expressed as:

$$dS_M = \left(\frac{\partial S_M}{\partial(\mu_0 H)} \right)_T d(\mu_0 H) + \left(\frac{\partial S_M}{\partial T} \right)_{(\mu_0 H)} dT \quad (2)$$

Taking into account one of the Maxwell's relations, namely that of $\left(\frac{\partial S_M}{\partial(\mu_0 H)} \right)_T = \left(\frac{\partial M}{\partial T} \right)_{(\mu_0 H)}$, and inserting it to Eq. 2, leads to:

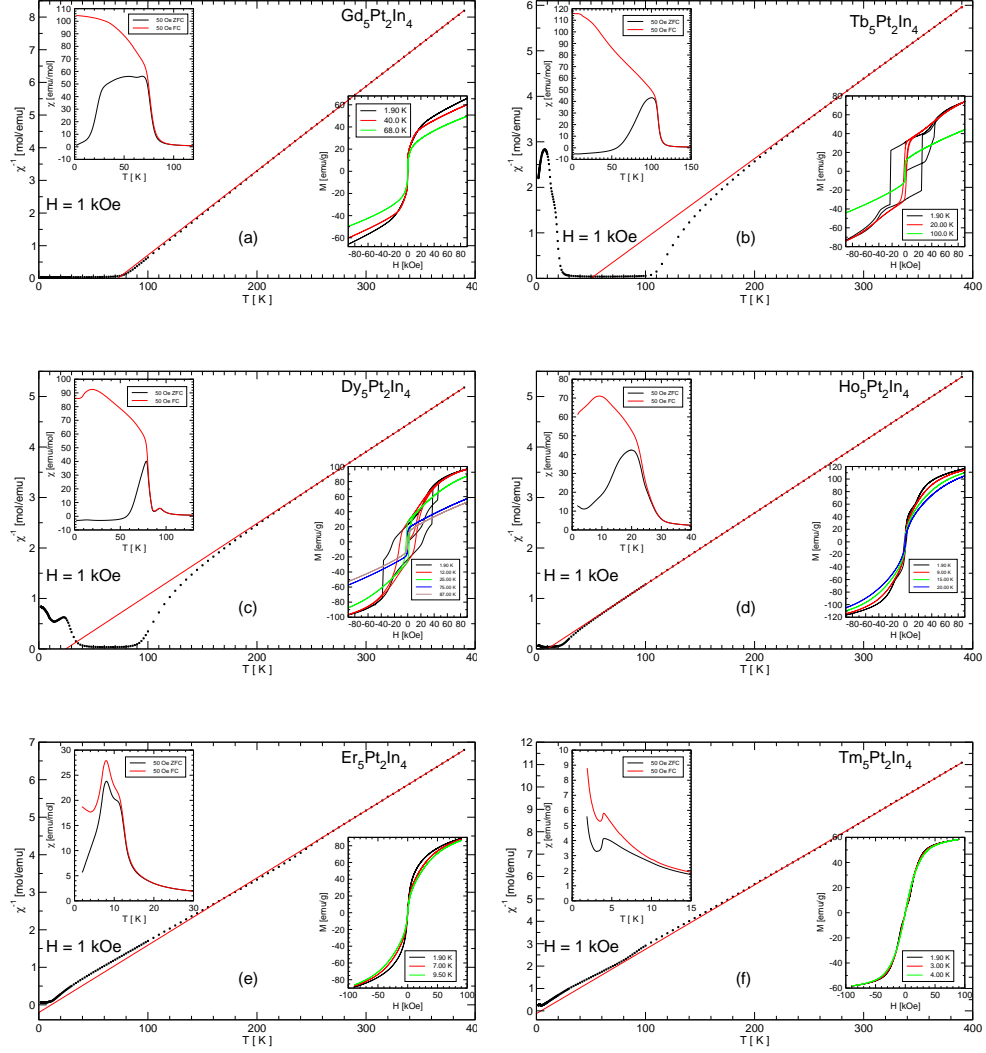


FIG. 3. Reciprocal magnetic susceptibility with the fitted line represents the Curie-Weiss law for $\text{RE}_5\text{Pt}_2\text{In}_4$: (a) $\text{RE} = \text{Gd}$, (b) $\text{RE} = \text{Tb}$, (c) $\text{RE} = \text{Dy}$ (d) $\text{RE} = \text{Ho}$, (e) $\text{RE} = \text{Er}$, and (f) $\text{RE} = \text{Tm}$. The low-temperature behavior measured at 50 Oe (ZFC and FC regimes) is shown in the upper insets, while the isothermal magnetization vs. external magnetic field at selected temperatures is presented in the lower insets.

$$dS_M = \left(\frac{\partial M}{\partial T} \right)_{(\mu_0 H)} d(\mu_0 H) + \left(\frac{\partial S_M}{\partial T} \right)_{(\mu_0 H)} dT \quad (3)$$

where M denotes magnetization.

By applying the isothermal condition ($dT = 0$) and integrating Eq. 3 over magnetic flux density, one gets:

$$\Delta S_M(T, \Delta \mu_0 H) = \int_0^{\mu_0 H_{max}} \left(\frac{\partial M(\mu_0 H, T)}{\partial T} \right)_{(\mu_0 H)} d\mu_0 H \quad (4)$$

where $\Delta \mu_0 H$ is a change of the magnetic flux density (usually calculated with respect to the initial flux equal

to zero), while $\left(\frac{\partial M(\mu_0 H, T)}{\partial T} \right)_{(\mu_0 H)}$ is a derivative of magnetization over temperature at fixed magnetic flux density of $\mu_0 H$. Details of mathematical formalism related to the magnetocaloric effect can be found for example in the book by Tishin and Spichkin [27].

Fig. 5 shows the magnetization vs. temperature $M(T)$ curves collected at a number of fixed magnetic flux density values up to 9 T for the $\text{RE}_5\text{Pt}_2\text{In}_4$ ($\text{RE} = \text{Gd-Tm}$) compounds. Based on the above data, the corresponding magnetic entropy changes have been calculated using Eq. 4. The results are presented in Fig. 6. Maximum entropy changes around corresponding magnetic transition temperatures reach 3.7, 3.4, 6.3, 11.8, 11.4, and 10.2 $\text{J}\cdot\text{kg}^{-1}\cdot\text{K}^{-1}$ under magnetic flux density change of 0–9 T for $\text{RE} = \text{Gd, Tb, Dy, Ho, Er, and Tm}$, re-

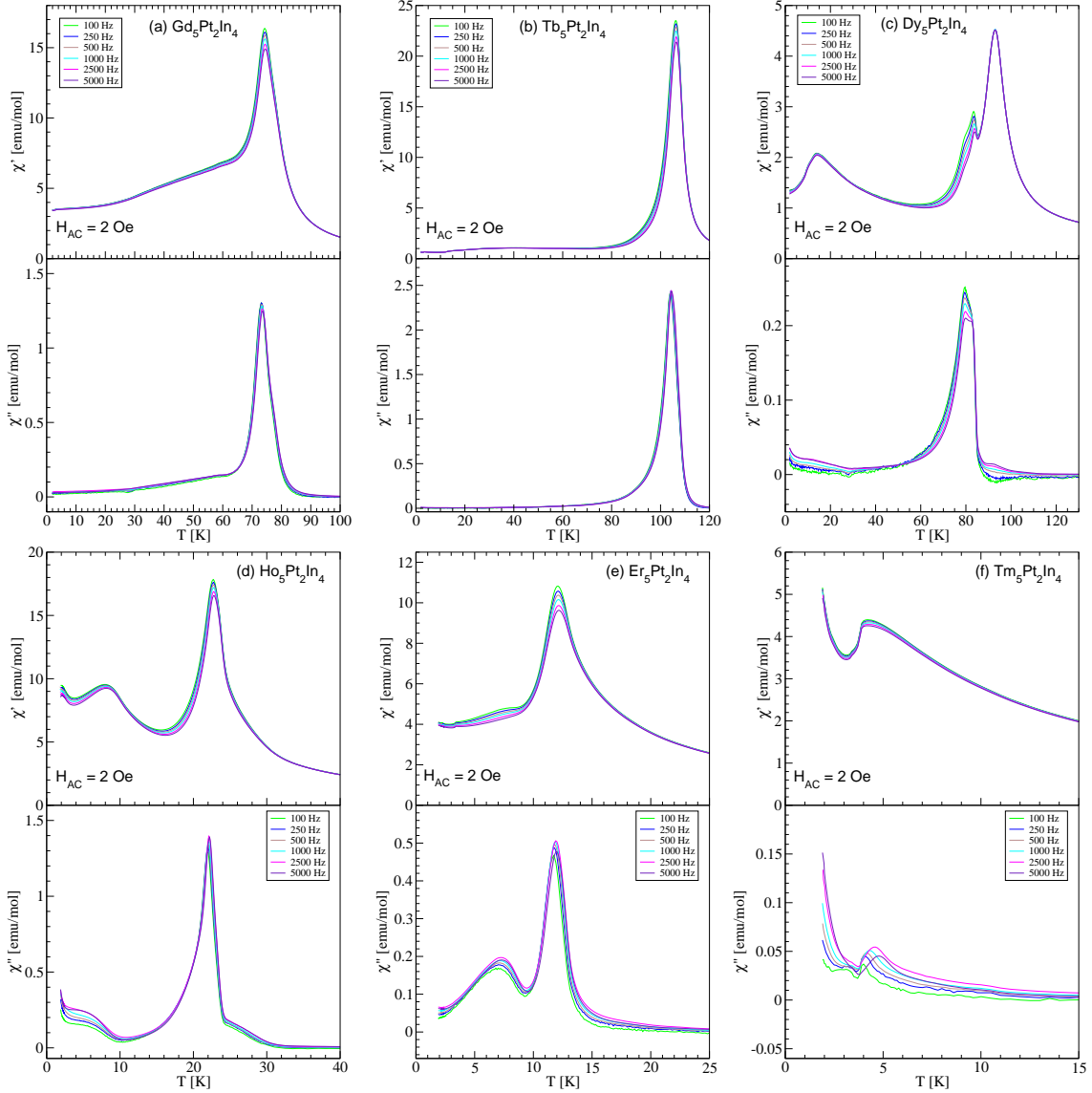


FIG. 4. AC magnetic susceptibility of $\text{RE}_5\text{Pt}_2\text{In}_4$: (a) $\text{RE} = \text{Gd}$, (b) $\text{RE} = \text{Tb}$, (c) $\text{RE} = \text{Dy}$ (d) $\text{RE} = \text{Ho}$, (e) $\text{RE} = \text{Er}$, and (f) $\text{RE} = \text{Tm}$ taken at frequencies between 100 Hz and 5000 Hz. χ' and χ'' refer to the real and imaginary components, respectively.

spectively. The values for other magnetic flux density changes are listed in Table III. The cases of $\text{Tb}_5\text{Pt}_2\text{In}_4$ and $\text{Dy}_5\text{Pt}_2\text{In}_4$ need an extra comment, as two distinct maxima are found in the magnetic entropy change vs. temperature plots (see Figs. 6b and 6c). The high-temperature maximum (~ 110 K for $\text{RE} = \text{Tb}$ and ~ 95 K for $\text{RE} = \text{Dy}$), which dominates for low magnetic flux density changes, corresponds to the transition from para to ferromagnetic state. The low-temperature maximum (~ 45 K for $\text{RE} = \text{Tb}$ and ~ 25 K for $\text{RE} = \text{Dy}$), which dominates for high magnetic flux density changes, indicates an extra transformation of the magnetic structure. The magnetic entropy changes corresponding to the low- and high-temperature maxima are shown separately in Figs. 6b and 6c.

The temperature averaged magnetic entropy change (TEC) is another parameter used for evaluating MCE. TEC is defined by the following formula [28]:

$$TEC(\Delta T_{\text{lift}}, \Delta\mu_0 H) = \frac{1}{\Delta T_{\text{lift}}} \max_{T_{\text{mid}}} \left\{ \int_{T_{\text{mid}} - \frac{\Delta T_{\text{lift}}}{2}}^{T_{\text{mid}} + \frac{\Delta T_{\text{lift}}}{2}} \Delta S_M(T, \Delta\mu_0 H) dT \right\} \quad (5)$$

where T_{mid} is the center temperature of the temperature span ΔT_{lift} . The value of T_{mid} is determined by finding the one that maximizes the integral appearing in Eq. 5. The TEC values of $\text{RE}_5\text{Pt}_2\text{In}_4$ ($\text{RE} = \text{Gd-Tm}$), calculated for the temperature spans of 3, 5 and 10 K, are

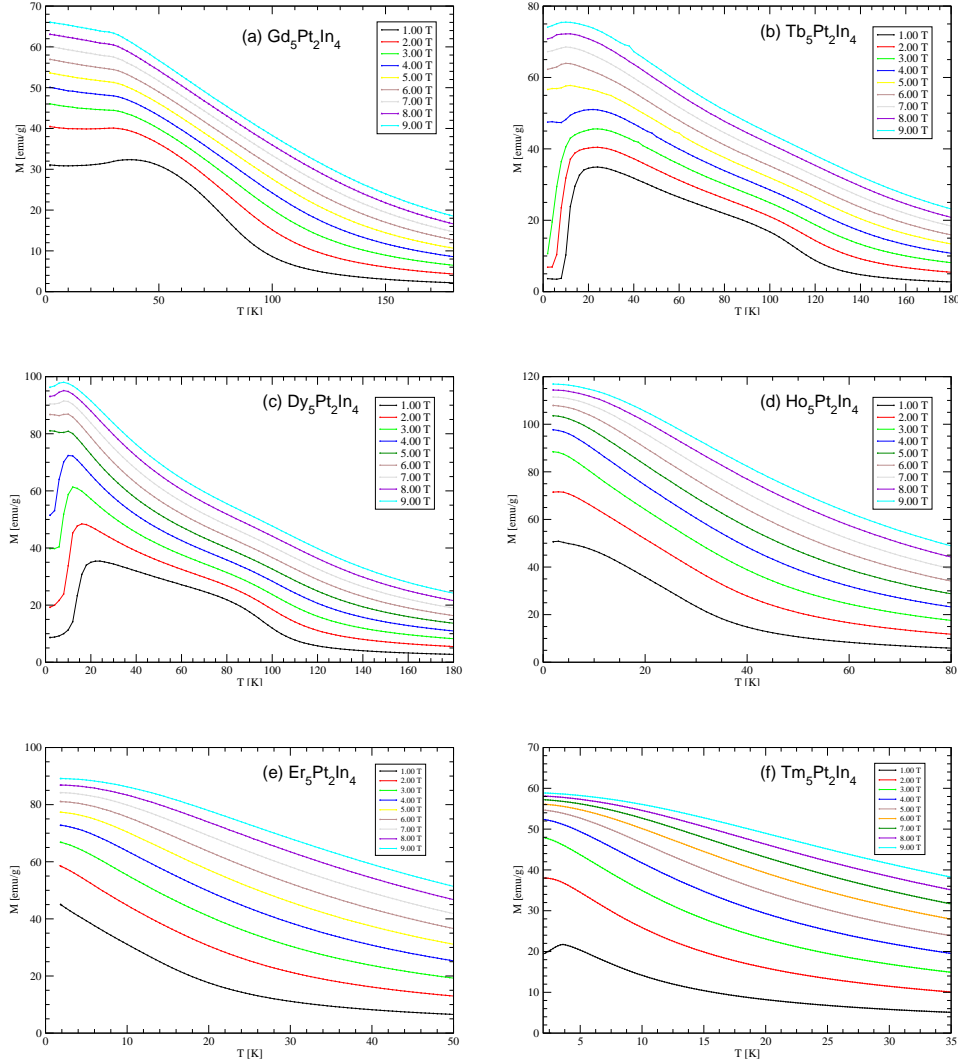


FIG. 5. Magnetization vs temperature curves under various magnetic flux density values up to 9 T for $\text{RE}_5\text{Pt}_2\text{In}_4$: (a) RE = Gd, (b) RE = Tb, (c) RE = Dy (d) RE = Ho, (e) RE = Er, and (f) RE = Tm.

presented in Fig. 7. It is worth noting that the TEC values for RE = Tb and Dy are always related to the dominating maximum, i.e. to the high-temperature maximum for the low magnetic flux density changes and the low-temperature one for the high magnetic flux density changes (see Figs. 7b and 7c).

b. Relative Cooling Power (RCP) and Refrigerant Capacity (RC)

Besides ΔS_M^{max} and TEC, the relative cooling power (RCP) [29] and refrigerant capacity (RC) [30] are another important parameters that can be used to assess the MCE performance. RCP is defined by the equation:

$$RCP = -\Delta S_M^{max} \times \delta T_{FWHM} \quad (6)$$

where δT_{FWHM} is the full width at half maximum of the

entropy change vs. temperature curve. RC is calculated from the following integral:

$$RC = \int_{T_1}^{T_2} |\Delta S_M| dT \quad (7)$$

where T_1 and T_2 denote the lower and upper limits of the FWHM temperature range, respectively.

Table III lists the determined values of RCP and RC for $\text{RE}_5\text{Pt}_2\text{In}_4$ (RE = Gd–Tm) under selected changes of magnetic flux densities. It is worth noting that for $\text{Dy}_5\text{Pt}_2\text{In}_4$, the RCP and RC values under magnetic flux density changes of 0–5 T are higher than those under 0–7 T. This unusual behavior is due to the fact that under $\Delta\mu_0 H = 0\text{--}5$ T, the low- and high-temperature maxima in $-\Delta S_M(T)$ are of similar heights and they overlap, leading to FWHM temperature interval being

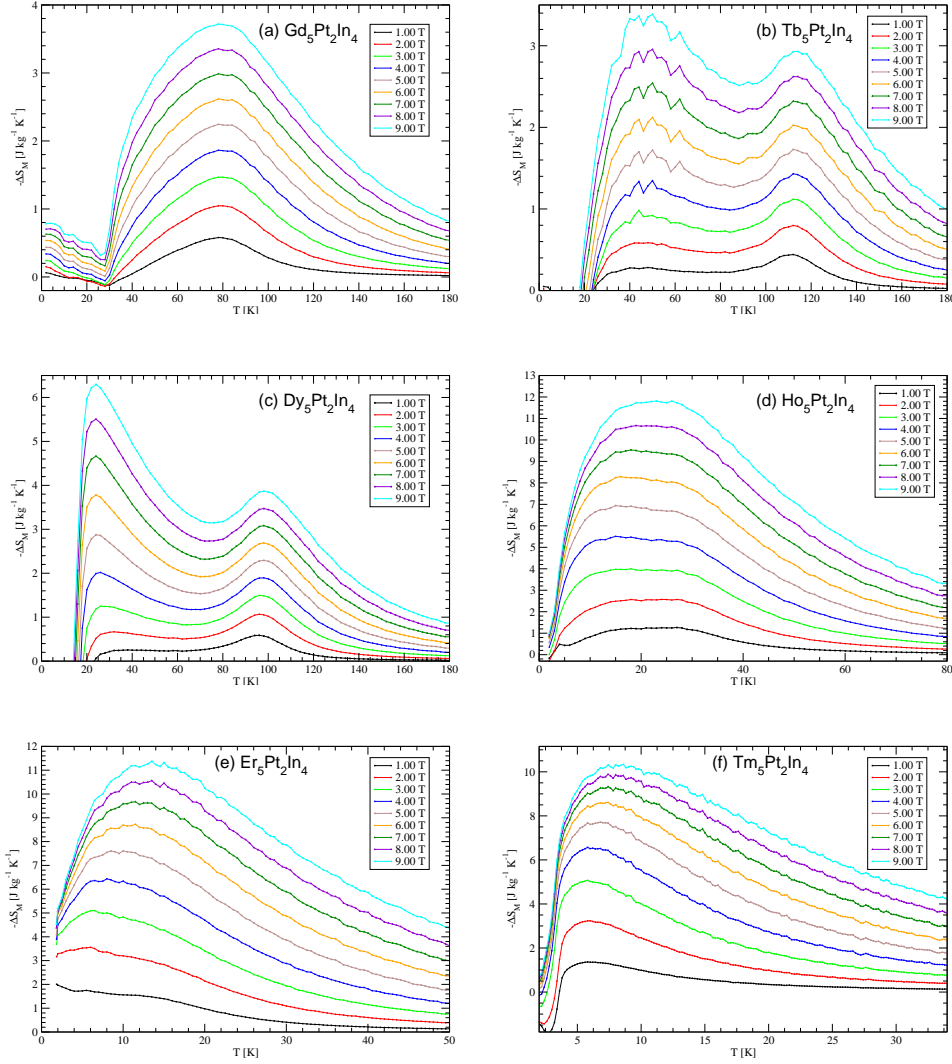


FIG. 6. Temperature dependence of the magnetic entropy change $-\Delta S_M^{max}$, as derived from the $M(H, T)$ data, under various magnetic flux density changes $\Delta\mu_0 H$ up to 0–9 T, for $RE_5Pt_2In_4$: (a) RE = Gd, (b) RE = Tb, (c) RE = Dy (d) RE = Ho, (e) RE = Er, and (f) RE = Tm.

TABLE III. The temperatures of maximum entropy change, maximum entropy changes $-\Delta S_M^{max}$ together with RCP and RC values under magnetic flux density changes $\Delta\mu_0 H = 0-2$ T, 0–5 T, 0–7 T and 0–9 T for the $RE_5Pt_2In_4$ (RE = Gd–Tm) and isostructural compounds.

Materials	Temp. for $-\Delta S_M^{max}$ [K]	$-\Delta S_M^{max} [J \cdot kg^{-1} \cdot K^{-1}]$				RCP [$J \cdot kg^{-1}$]				RC [$J \cdot kg^{-1}$]				Ref.
		0–2 T	0–5 T	0–7 T	0–9 T	0–2 T	0–5 T	0–7 T	0–9 T	0–2 T	0–5 T	0–7 T	0–9 T	
Dy ₅ Ni ₂ In ₄	19	1.8	3.6	4.7	-	49	178	286	-	37	130	209	-	[10]
Ho ₅ Ni ₂ In ₄	103	2.6	7.1	10.1	-	84	298	458	-	66	234	352	-	[10]
Er ₅ Ni ₂ In ₄	20	3.3	7.7	10.2	-	71	248	377	-	52	180	273	-	[10]
Gd ₅ Pt ₂ In ₄	78	1.0	2.2	3.0	3.7	58	172	261	359	48	139	209	290	this work
Tb ₅ Pt ₂ In ₄	45, 110	0.8	1.7	2.5	3.4	82	198	303	428	57	165	248	340	this work
Dy ₅ Pt ₂ In ₄	25, 95	1.1	2.9	4.7	6.3	45	290	250	363	33	201	180	263	this work
Ho ₅ Pt ₂ In ₄	23	2.5	6.9	9.5	11.8	94	302	451	607	82	254	373	495	this work
Er ₅ Pt ₂ In ₄	14	3.6	7.5	9.6	11.4	79	218	328	434	63	175	256	341	this work
Tm ₅ Pt ₂ In ₄	8	3.2	7.7	9.2	10.2	34	125	189	260	27	98	150	205	this work

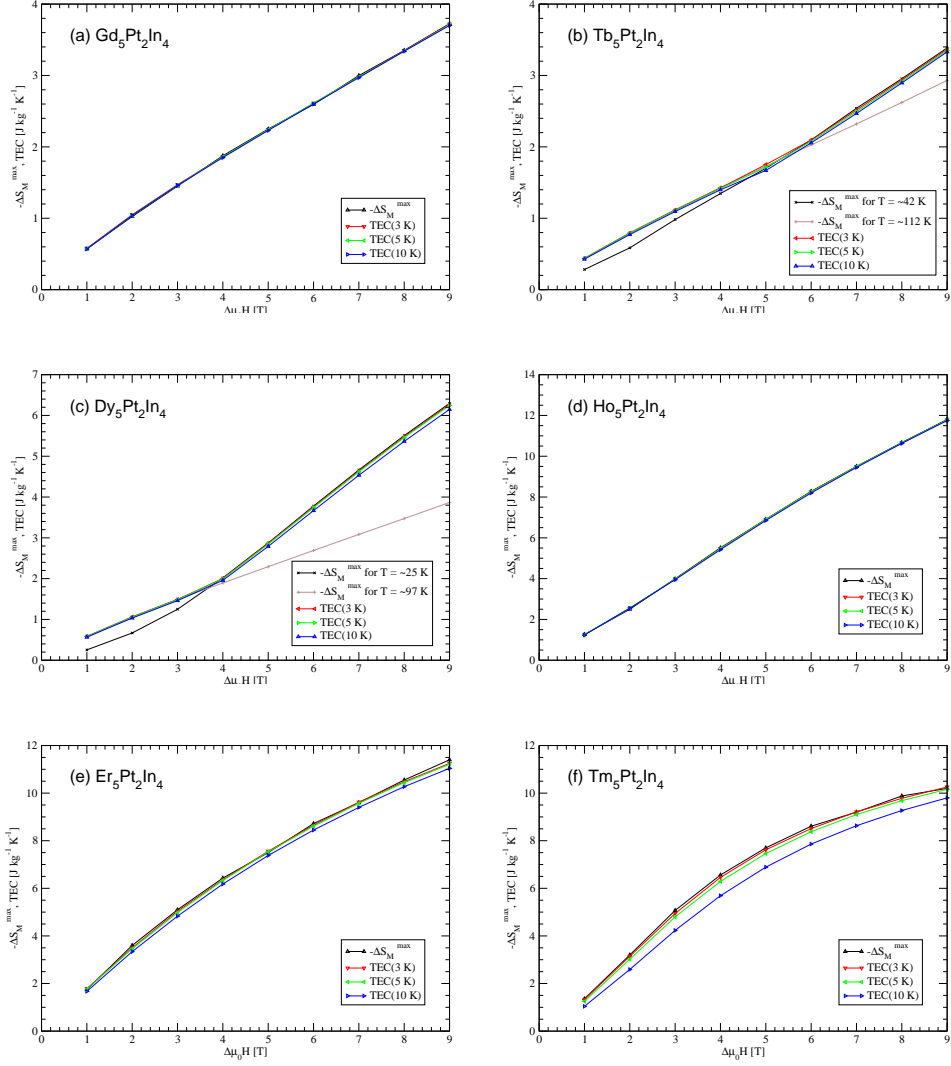


FIG. 7. The values of $-\Delta S_M^{max}$, TEC(3 K), TEC(5 K), and TEC(10 K) under various magnetic flux density changes $\Delta\mu_0H$ up to 0–9 T for $RE_5Pt_2In_4$: (a) RE = Gd, (b) RE = Tb, (c) RE = Dy, (d) RE = Ho, (e) RE = Er, and (f) RE = Tm, respectively. For RE = Tb and Dy, the magnetic entropy changes corresponding to the low- and high-temperature maxima are indicated by black and brown lines, respectively.

significantly wider than the one at higher magnetic flux density changes where low-temperature maximum dominates.

IV. DISCUSSION

This work reports the results of X-ray, DC, and AC magnetic measurements for the $RE_5Pt_2In_4$ (RE = Gd–Tm) compounds. The X-ray diffraction data confirm that $RE_5Pt_2In_4$ (RE = Gd–Tm) have an orthorhombic crystal structure of the $Lu_5Ni_2In_4$ -type. The crystal structure is a typical two-layered one with layers formed by the rare earth atoms ($z = 0$) separated by layers containing the remaining Pd and In atoms ($z = \frac{1}{2}$). The

refined lattice parameters and atomic coordinates, presented in Table I, are in good agreement with the previously reported ones [2].

The results of magnetometric measurements reveal that all investigated compounds order magnetically with decreasing temperature. The shapes of the magnetic susceptibility vs. temperature curves (see Figs. 3, 4) suggest para- to ferromagnetic transition for RE = Gd, Tb, Ho and Er, while for RE = Tm a para- to antiferromagnetic transition is found. The case of RE = Dy is more complicated as the ferromagnetic state is reached through an intermediate antiferromagnetic state occurring in relatively narrow temperature range. Anomalies in the $\chi(T)$ curves, observed below the respective critical temperatures of magnetic ordering for all compounds except

RE = Tm, suggest presence of additional temperature-induced magnetic transitions. Such a behavior has been observed in the isostructural $\text{RE}_5\text{Ni}_2\text{In}_4$ [4–10]. It can be attributed to complexity of the crystal structure as the rare earth atoms occupy three nonequivalent Wyckoff sites, which leads to competition of different interactions. Complex magnetic properties manifest themselves also in coexistence of the ferro- and antiferromagnetic contributions to the magnetic structure, as confirmed by the shapes of the magnetization vs. applied magnetic field curves, which show both presence of coercivity fields characteristic of ferromagnetic order as well as metamagnetic transitions characteristic of antiferromagnetic ordering (see the lower insets in Figs. 3a-f). It has to be mentioned that the exact thermal evolution of the magnetic structures cannot be determined solely from the magnetic data, but further neutron diffraction studies are required.

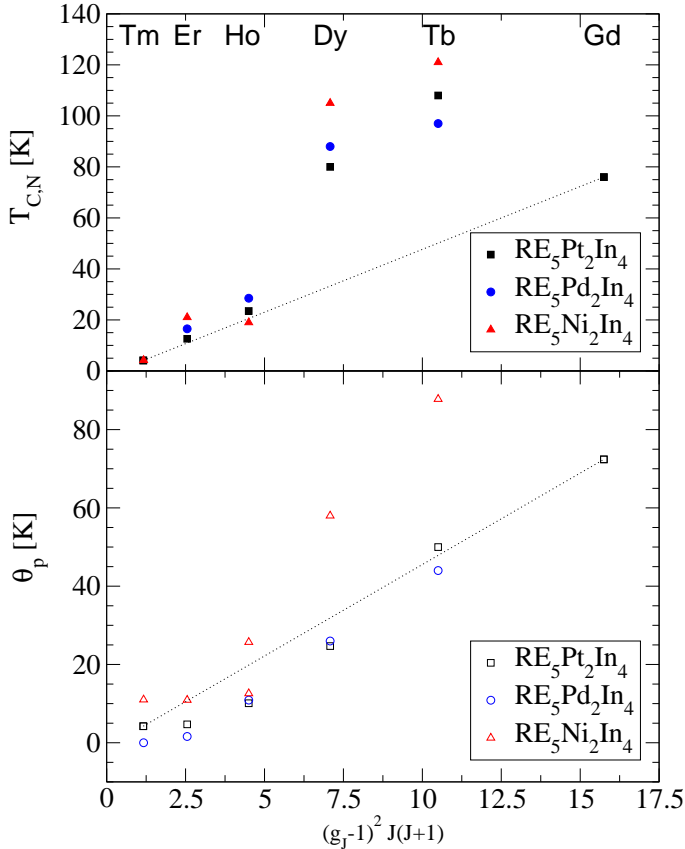


FIG. 8. Critical temperatures of magnetic ordering ($T_{C,N}$) along with paramagnetic Curie temperatures θ_p vs. de Gennes factor for $\text{RE}_5\text{T}_2\text{In}_4$ (RE = rare earth element, T = Ni, Pd, Pt). The data for T = Ni have been taken after [4–6, 8, 9], while those for T = Pd after [11]. The dotted lines indicate theoretical de Gennes scaling for $\text{RE}_5\text{Pt}_2\text{In}_4$ while taking the characteristic temperatures of $\text{Gd}_5\text{Pt}_2\text{In}_4$ as reference.

Reciprocal magnetic susceptibilities of $\text{RE}_5\text{Pt}_2\text{In}_4$ (RE = Tb-Tm) follow the Curie-Weiss law at high tempera-

tures (see Fig. 3). The deviations from linearity, as observed at lower temperatures, indicate influence of the crystalline electric field (CEF). The determined Curie temperatures are positive revealing that the ferromagnetic interactions are dominant. The obtained values of the effective magnetic moments are close to those predicted for the free RE^{3+} ions. Small discrepancies between the experimental and theoretical values do not exceed systematic errors of the experiment. Therefore the magnetism of $\text{RE}_5\text{Pt}_2\text{In}_4$ (RE = Tb-Tm) is strictly related to the rare earth magnetic moments, while the magnetic moments of the remaining Pt and In elements are either zero or they are too small to be detectable when accompanied by high rare earth moments.

According to the crystallographic data reported in Tables 1 and 4 in [2], the rare earth interatomic distances in $\text{RE}_5\text{Pt}_2\text{In}_4$ (RE = Tb-Tm) exceed 3.3 Å. Therefore, they are high enough to exclude any direct interactions and the indirect interactions of the RKKY-type are expected in this family of compounds. One of the predictions of the RKKY theory is so called de Gennes scaling, which assumes direct proportionality between the critical temperature of magnetic ordering and the de Gennes factor defined as $(g_J - 1)^2 J(J + 1)$, where g is a Landé factor, while J is a total angular momentum of the RE^{3+} rare earth ion. Figure 8 presents the critical temperatures of magnetic ordering for $\text{RE}_5\text{T}_2\text{In}_4$ (T = Ni, Pd, Pt) plotted against de Gennes factor. In addition, the paramagnetic Curie temperatures, which are also a measure of the strength of magnetic interactions, are shown. The lack of theoretically predicted proportionality is yet another evidence of significant influence of CEF on magnetic properties of $\text{RE}_5\text{T}_2\text{In}_4$ (RE = rare earth element, T = Ni, Pd, Pt). It is worth noting that the critical temperature of magnetic ordering of a particular Ni-based compound is in the most cases higher than those of its Pd- and Pt-based analogues. This finding coincides with increase of the interatomic distances due to increasing number of the atomic number of the d-electron element (compare the lattice parameters for T = Ni [3, 5, 31], Pd [32] and Pt [2]). Therefore, the increase of the interatomic distances leads to weaken the magnetic interactions.

The type of magnetic transition (the first or second order) can be derived from shapes of the Arrott plots (M^2 vs. $\mu_0 H/M$) collected at selected temperatures [33]. Positive slope of the Arrott curve corresponds to the second order phase transitions (SOPT), while the negative slope to the first order phase transitions (FOPT). Fig 9 shows the Arrott plots for $\text{RE}_5\text{Pt}_2\text{In}_4$ (RE = Gd-Tm). For RE = Gd, Ho, Er and Tm only positive slopes are found, indicating magnetic transition of the second order type. The situation is more complicated for RE = Tb and Dy, as positive slopes characteristic of SOPT are found below the critical temperature of magnetic ordering, except the lowest temperature of 2 K, where positive slope characteristic of FOPT is observed within limited range. This behavior is consistent with the shapes of the magnetiza-

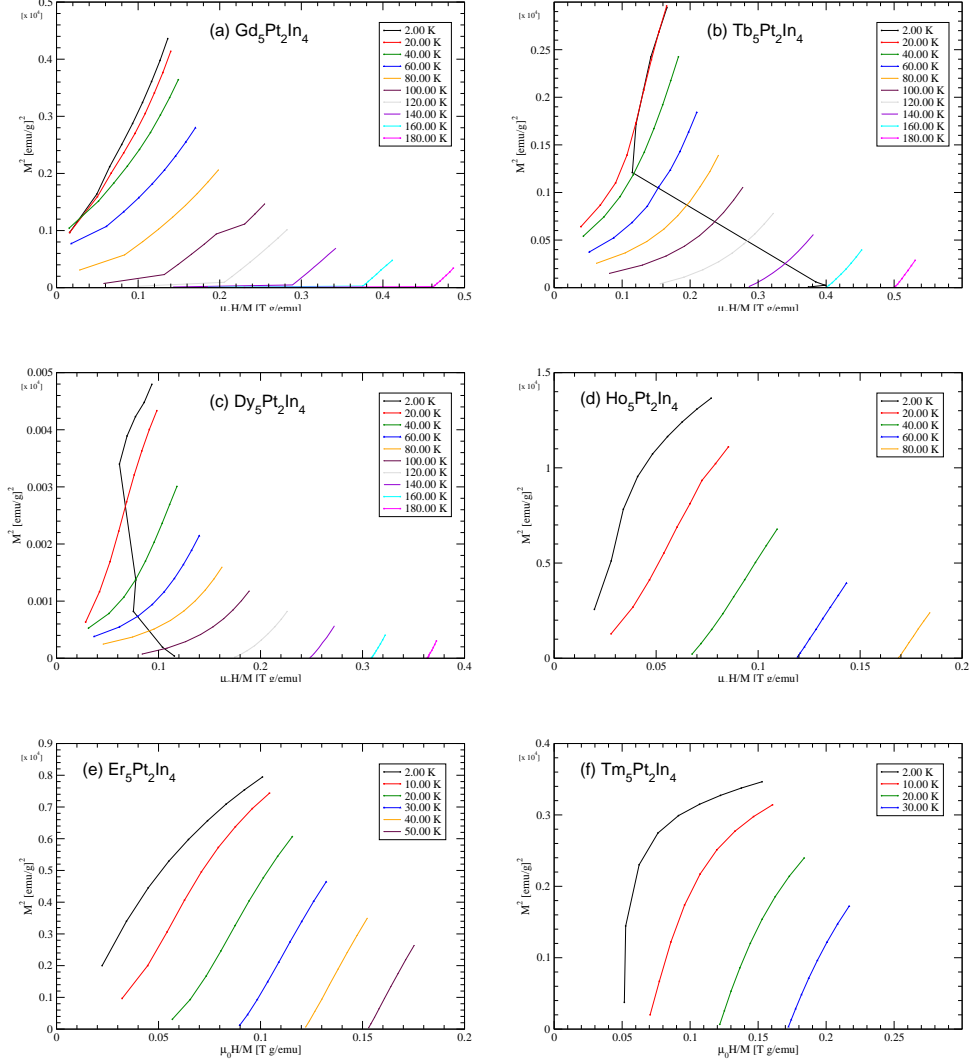


FIG. 9. The plots of M^2 versus $\mu_0 H/M$ at selected temperatures for $RE_5Pt_2In_4$: (a) RE = Gd, (b) RE = Tb, (c) RE = Dy (d) RE = Ho, (e) RE = Er and (f) RE = Tm.

tion vs. temperature curves (see Fig. 5). For the low values of the applied magnetic field, magnetization initially increases with decreasing temperature, but finally undergoes a sudden drop below 20 K. Such a behavior indicates that the high-temperature ferro-/ferrimagnetic structure transforms into an antiferromagnetic one with decreasing temperature. According to the shape of Arrott plots this phase transition is of the first order type (FOPT).

Table IV contains comparison of the MCE performance under magnetic flux density change of 0-7 T for $RE_5Pt_2In_4$ (RE = Gd-Tm), isostructural $RE_5Ni_2In_4$ (RE = Dy, Ho, Er) and other selected ternary rare earth-based indides. For a selected rare earth element, the MCE performance of a member of the $RE_5Pt_2In_4$ (RE = Gd-Tm) family of compounds shows similar perfor-

mance to that of its $RE_5Ni_2In_4$ and $RE_{11}T_4In_9$ (T = Co, Ni) analogues. It is worth mentioning that the MCE performance of $RE_5Pt_2In_4$ (RE = Ho and Er), which is reported in this work, is quite high and comparable to that of the best known low-temperature magnetocaloric materials [10, 12–22, 34, 36, 37, 39, 40].

V. CONCLUSIONS

The $RE_5Pt_2In_4$ (RE = Gd-Tm) compounds crystallize in an orthorhombic crystal structure of the the $Lu_5Ni_2In_4$ -type ($Pbam$ space group) in which the rare earth atoms occupy three nonequivalent sites. The compounds show complex magnetic properties and quite good MCE performance at low temperatures. With

TABLE IV. Comparison of the magnetocaloric performance under magnetic flux density change of 0-7 T for RE₅Pt₂In₄ (RE = Gd-Tm), isostructural RE₅Ni₂In₄ (RE = Dy, Ho, Er) and other selected ternary rare earth-based indides. T_{cr} denotes critical temperature of the magnetic ordering (Curie or Néel temperature).

Material	T_{cr} [K]	$-\Delta S_M^{\max}$ [J·kg ⁻¹ ·K ⁻¹]	RCP [J·kg ⁻¹]	RC [J·kg ⁻¹]	Ref.
Gd ₅ Pt ₂ In ₄	76	3.0	261	209	this work
Tb ₅ Pt ₂ In ₄	108	2.5	303	248	this work
Dy ₅ Pt ₂ In ₄	93	4.7	250	180	this work
Ho ₅ Pt ₂ In ₄	23.5	9.5	451	373	this work
Er ₅ Pt ₂ In ₄	12.6	9.6	328	256	this work
Tm ₅ Pt ₂ In ₄	4.1	9.2	189	150	this work
Dy ₅ Ni ₂ In ₄	105	4.7	286	209	[10]
Ho ₅ Ni ₂ In ₄	31	10.1	458	352	[10]
Er ₅ Ni ₂ In ₄	21	10.2	377	273	[10]
Gd ₁₁ Co ₄ In ₉	86	10.95	538.1	405.9	[34]
Tb ₁₁ Co ₄ In ₉	95*	4.43	376.8	274.4	[35]
Dy ₁₁ Co ₄ In ₉	37	4.66	213.9	165.9	[34]
Ho ₁₁ Co ₄ In ₉	20	12.29	475.2	357.4	[34]
Er ₁₁ Co ₄ In ₉	5.4*	12.80	416.1	320.0	[35]
Gd ₁₁ Ni ₄ In ₉	91	3.58	269.0	206.4	[36]
Dy ₁₁ Ni ₄ In ₉	18	6.02	194.9	144.7	[36]
Ho ₁₁ Ni ₄ In ₉	13.5	12.44	353.0	269.2	[36]
Gd ₆ Co _{2.2} In _{0.8}	76	11.84	814.23	633.55	[37]
Tb ₆ Co _{2.2} In _{0.8}	32	8.96	394.15	284.32	[37]
Dy ₆ Co _{2.2} In _{0.8}	50	9.59	517.01	389.77	[37]
Ho ₆ Co _{2.2} In _{0.8}	18	20.83	626.36	466.07	[37]

* after [38]

decreasing temperature all investigated compounds undergo a transition to magnetically ordered state, in the most cases followed by a cascade of extra magnetic transitions appearing below the respective critical temperature of magnetic ordering. The rare earth atoms are found to possess magnetic moments, while the moments of the remaining Pt and In atoms are absent or are too small to be detected while accompanied by the strong rare earth's moments. The MCE performance of RE₅Pt₂In₄ (RE = Gd-Tm) is comparable to that of the best known low-temperature magnetocaloric materials, especially while taking into account the compounds with RE = Ho and Er.

DECLARATION OF COMPETING INTEREST

The authors declare no conflict of interest.

ACKNOWLEDGEMENTS

This research was supported in part by the Excellence Initiative – Research University Program at the Jagiellonian University in Kraków. The research was partially carried out with the equipment purchased thanks to the financial support of the European Regional Development Fund in the framework of the Polish Innovation Economy Operational Program (contract no.POIG.02.01.00-12-023/08).

[1] S. Gupta, K. Suresh, Review on magnetic and related properties of RTX compounds, Journal of Alloys and Compounds 618 (2015) 562–606. doi:10.1016/j.jallcom.2014.08.079.

[2] R. Zaremba, Ute Ch. Rodewald, R. Pöttgen, Rare Earth-Rich Indides RE₅Pt₂In₄ (RE = Sc, Y, La–Nd, Sm, Gd–Tm, Lu), Monatshefte für Chemie 138 (2007) 819–822. doi:10.1007/s00706-007-0702-6.

- [3] V. I. Zaremba, Ya. M. Kalychak, P. Yu. Zavaliy, V. A. Bruskov, Crystal structures of the compounds $R_5Ni_2In_4$ ($R = Ho, Er, Tm, Lu$), *Kristallografiya* 36 (1991) 1415–1418.
- [4] Yu. B. Tyvanchuk, B. Penc, A. Szytuła, A. Zarzycki, Magnetic Properties of $Ho_5Ni_2In_4$, *Acta Phys. Pol. A* 117 (2010) 599–600. doi:10.12693/APhysPolA.117.599.
- [5] A. Provino, Y. Mudryk, D. Paudyal, P. V. Smetana, V. K. Pecharsky, K. A. Gschneidner, Jr., J. D. Corbett, Crystal structure of $Tb_5Ni_2In_4$ and $Y_5Ni_2In_4$, and magnetic properties of $Dy_5Ni_2In_4$, *J. Appl. Phys.* 111 (2012) 07E122. doi:10.1063/1.3673432.
- [6] Ł. Gondek, J. Przewoźnik, J. Czub, Yu. Tyvanchuk, A. Szytuła, A. Arulraj, Crystal and magnetic properties of $Er_5Ni_2In_4$ at low temperatures, *Intermetallics* 21 (2012) 10–17. doi:10.1016/j.intermet.2011.09.007.
- [7] A. Szytuła, Yu. Tyvanchuk, S. Baran, J. Przewoźnik, Ya. M. Kalychak, Magnetic and thermal properties of $Tm_5Ni_2In_4$, *Intermetallics* 43 (2013) 99–102. doi:10.1016/j.intermet.2013.07.014.
- [8] A. Szytuła, S. Baran, D. Kaczorowski, W. Sikora, A. Hoser, Magnetic ordering in $Tm_5Ni_2In_4$, *Journal of Alloys and Compounds* 617 (2014) 149–153. doi:10.1016/j.jallcom.2014.07.190.
- [9] C. Ritter, A. Provino, P. Manfrinetti, V. K. Pecharsky, K. A. Gschneidner, S. K. Dhar, Magnetic structures of $R_5Ni_2In_4$ and $R_{11}Ni_4In_9$ ($R = Tb$ and Ho): strong hierarchy in the temperature dependence of the magnetic ordering in the multiple rare-earth sublattices, *Journal of Physics: Condensed Matter* 27 (2015) 476001. doi:10.1088/0953-8984/27/47/476001.
- [10] Z. Zhang, X. Dong, Q. Wang, L. Li, Investigation of the crystal structure, magnetic phase transition and magnetocaloric effect in $RE_5Ni_2In_4$ ($RE = Dy, Ho$ and Er) compounds, *Intermetallics* 100 (2018) 136–141. doi:10.1016/j.intermet.2018.06.012.
- [11] S. Baran, A. Deptuch, M. Reehuis, Y. Tyvanchuk, F. Yokaichiya, A. Szytuła, Complex magnetic ordering in $RE_5Pd_2In_4$ ($RE = Tb-Tm$) compounds investigated by neutron diffraction and magnetometric measurements, *Journal of Alloys and Compounds* 877 (2021). doi:10.1016/j.jallcom.2021.160171.
- [12] L. Li, M. Yan, Recent progress in the development of $RE_2TMTM'O_6$ double perovskite oxides for cryogenic magnetic refrigeration, *Journal of Materials Science & Technology* 136 (2023) 1–12. doi:10.1016/j.jmst.2022.01.041.
- [13] D. Guo, L. M. Moreno-Ramírez, J.-Y. Law, Y. Zhang, V. Franco, Excellent cryogenic magnetocaloric properties in heavy rare-earth based $HRENiGa_2$ ($HRE = Dy, Ho$, or Er) compounds, *Science China Materials* (2022). doi:10.1007/s40843-022-2095-6.
- [14] P. Xu, L. Hu, Z. Zhang, H. Wang, L. Li, Electronic structure, magnetic properties and magnetocaloric performance in rare earths (RE) based RE_2BaZnO_5 ($RE = Gd, Dy, Ho$, and Er) compounds, *Acta Materialia* 236 (2022) 118114. doi:10.1016/j.actamat.2022.118114.
- [15] Y. Zhang, S. Li, L. Hu, X. Wang, L. Li, M. Yan, Excellent magnetocaloric performance in the carbide compounds $RE_2Cr_2C_3$ ($RE = Er, Ho$, and Dy) and their composites, *Materials Today Physics* 27 (2022) 100786. doi:10.1016/j.mtphys.2022.100786.
- [16] Z. Ma, X. Dong, Z. Zhang, L. Li, Achievement of promising cryogenic magnetocaloric performances in $La_{1-x}Pr_xFe_{12}B_6$ compounds, *Journal of Materials Science & Technology* 92 (2021) 138–142. doi:10.1016/j.jmst.2021.02.055.
- [17] Y. Zhang, Review of the structural, magnetic and magnetocaloric properties in ternary rare earth RE_2T_2X type intermetallic compounds, *Journal of Alloys and Compounds* 787 (2019) 1173–1186. doi:10.1016/j.jallcom.2019.02.175.
- [18] L. Li, M. Yan, Recent progresses in exploring the rare earth based intermetallic compounds for cryogenic magnetic refrigeration, *Journal of Alloys and Compounds* 823 (2020) 153810. doi:10.1016/j.jallcom.2020.153810.
- [19] Y. Zhang, Y. Tian, Z. Zhang, Y. Jia, B. Zhang, M. Jiang, J. Wang, Z. Ren, Magnetic properties and giant cryogenic magnetocaloric effect in B-site ordered antiferromagnetic Gd_2MgTiO_2 double perovskite oxide, *Acta Materialia* 226 (2022) 117669. doi:10.1016/j.actamat.2022.117669.
- [20] P. Xu, Z. Ma, P. Wang, H. Wang, L. Li, Excellent cryogenic magnetocaloric performances in ferromagnetic Sr_2GdNbO_6 double perovskite compound, *Materials Today Physics* 20 (2021) 100470. doi:10.1016/j.mtphys.2021.100470.
- [21] L. Li, P. Xu, S. Ye, Y. Li, G. Liu, D. Huo, M. Yan, Magnetic properties and excellent cryogenic magnetocaloric performances in b-site ordered RE_2ZnMnO_6 ($RE = Gd, Dy$ and Ho) perovskites, *Acta Materialia* 194 (2020) 354–365. doi:10.1016/j.actamat.2020.05.036.
- [22] Y. Zhang, J. Zhu, S. Li, J. Wang, Z. Ren, Achievement of giant cryogenic refrigerant capacity in quinary rare-earths based high-entropy amorphous alloy, *Journal of Materials Science & Technology* 102 (2022) 66–71. doi:10.1016/j.jmst.2021.06.028.
- [23] J. Rodríguez-Carvajal, Recent advances in magnetic structure determination by neutron powder diffraction, *Physica B* 192 (1993) 55–69. doi:10.1016/0921-4526(93)90108-I.
- [24] J. Rodríguez-Carvajal, Recent developments of the program fullprof, *Newsletter of the Commission for Powder Diffraction of the IUCr* 26 (2001) 12–19.
- [25] K. Momma, F. Izumi, *VESTA3* for three-dimensional visualization of crystal, volumetric and morphology data, *Journal of Applied Crystallography* 44 (2011) 1272–1276. doi:10.1107/S0021889811038970.
- [26] C. Kittel, *Introduction to Solid State Physics* 8th ed., John Wiley and Sons, New Jersey, America, 2004.
- [27] A. M. Tishin, Y. I. Spichkin, *The Magnetocaloric Effect and its Applications*, Institute of Physics Publishing, Bristol and Philadelphia, 2003.
- [28] L. D. Griffith, Y. Mudryk, J. Slaughter, V. K. Pecharsky, Material-based figure of merit for caloric materials, *J. Appl. Phys.* 123 (2018) 034902. doi:10.1063/1.5004173.
- [29] K. A. Gschneidner, Jr., V. K. Pecharsky, Magnetocaloric materials, *Annu. Rev. Mater. Sci.* 30 (2000) 387–429. doi:10.1146/annurev.matsci.30.1.387.
- [30] M. E. Wood, W. H. Potter, General analysis of magnetic refrigeration and its optimization using a new concept: maximization of refrigerant capacity, *Cryogenics* 25 (1985) 667–683. doi:10.1016/0011-2275(85)90187-0.
- [31] Yu. B. Tyvanchuk, U. C. Rodewald, Ya. M. Kalychak, R. Pöttgen, Rare earth–nickel–indides $Dy_5Ni_2In_4$ and $RE_4Ni_{11}In_{20}$ ($RE = Gd, Tb, Dy$), *Journal of Solid State Chemistry* 181 (2008) 878–883. doi:10.1016/j.jssc.2008.01.035.

- [32] L. Sojka, M. Dashkevych, B. Belan, M. Manyako, V. Davydov, L. Akselrud, Ya. M. Kalychak, Crystal structure of alloys $R_5Pd_2In_4$ ($R = Y, Tb, Dy, Ho, Er, Tm, Lu$), *Ukr. Chem. J.* 74 (2008) 90–94.
- [33] B. K. Banerjee, On a generalised approach to first and second order magnetic transitions, *Phys. Lett.* 12 (1964) 16–17. doi:10.1016/0031-9163(64)91158-8.
- [34] Z. Zhang, P. Wang, N. Wang, X. Wang, P. Xu, L. Li, Structural and cryogenic magnetic properties of rare earth rich $RE_{11}Co_4In_9$ ($RE = Gd, Dy$ and Ho) intermetallic compounds, *Dalton Trans.* 49 (2020) 8764–8773. doi:10.1039/D0DT01212B.
- [35] S. Baran, A. R. Hayyu, Yu. Tyvanchuk, A. Szytuła, Magnetocaloric performance of $RE_{11}Co_4In_9$ ($RE = Tb, Er$), *Phase Transitions* 96 (2023) 115–125. doi:10.1080/01411594.2022.2149398.
- [36] Z. Zhang, P. Wang, Y. Jia, X. Wang, L. Li, Crystal structure, magnetic phase transitions and magnetocaloric effect (MCE) in layer-like $RE_{11}Ni_4In_9$ ($RE = Gd, Dy$ and Ho) compounds, *Journal of Alloys and Compounds* 851 (2021) 155863. doi:10.1016/j.jallcom.2020.155863.
- [37] Z. Zhang, I. Muts, L. Li, R. Pöttgen, Magnetic properties and magnetocaloric performances of the rare earth-rich intermetallics $RE_6Co_2In_{0.8}$ ($RE = Gd, Tb, Dy$ and Ho) with Ho_6Co_2Ga -type structure, *Intermetallics* 136 (2021) 107254. doi:10.1016/j.intermet.2021.107254.
- [38] S. Baran, Yu. Tyvanchuk, A. Szytuła, Crystal structure and magnetic properties of $R_{11}Co_4In_9$ ($R = Tb, Dy, Ho$ and Er) compounds, *Intermetallics* 130 (2021) 107065. doi:10.1016/j.intermet.2020.107065.
- [39] K. A. Gschneidner, Jr., V. K. Pecharsky, A. O. Tsokol, Recent developments in magnetocaloric materials, *Rep. Prog. Phys.* 68 (2005) 1479–1539. doi:10.1088/0034-4885/68/6/R04.
- [40] J. Lyubina, Magnetocaloric materials for energy efficient cooling, *Journal of Physics D: Applied Physics* 50 (2017) 053002. doi:10.1088/1361-6463/50/5/053002.